Self diffusion of interacting membrane proteins

James R. Abney,*§ Bethe A. Scalettar,‡§ and John C. Owicki*§
*Cell and Molecular Biology Division and ‡Chemical Biodynamics Division, Lawrence Berkeley Laboratory, Berkeley, California 94720; and §Department of Biophysics and Medical Physics, University of California, Berkeley, California 94720

ABSTRACT A two-dimensional version of the generalized Smoluchowski equation is used to analyze the time (or distance) dependent self diffusion of interacting membrane proteins in concentrated membrane systems. This equation provides a well established starting point for descriptions of the diffusion of particles that interact through both direct and hydrodynamic forces; in this initial work only the effects of direct interactions are explicitly considered. Data describing diffusion in the presence of hard-core repulsions, soft repulsions, and soft repulsions with weak attractions are presented. The effect that interactions have on the self-diffusion coefficient of a real protein molecule from mouse liver gap junctions is also calculated. The results indicate that self diffusion is always inhibited by direct interactions; this observation is interpreted in terms of the caging that will exist at finite protein concentration. It is also noted that, over small distance scales, the diffusion coefficient is determined entirely by the very strong Brownian forces; therefore, as a function of displacement the self-diffusion coefficient decays (rapidly) from its value at infinite dilution to its steady-state interaction-averaged value. The steady-state self-diffusion coefficient describes motion over distance scales that range from ~10 nm to cellular dimensions and is the quantity measured in fluorescence recovery after photobleaching experiments. The short-ranged behavior of the diffusion coefficient is important on the interparticle-distance scale and may therefore influence the rate at which nearest-neighbor collisional processes take place. The hard-disk theoretical results presented here are in excellent agreement with lattice Monte-Carlo results obtained by other workers. The concentration dependence of experimentally measured diffusion coefficients of antibody-hapten complexes bound to the membrane surface is consistent with that predicted by the theory. The variation in experimental diffusion coefficients of integral membrane proteins is greater than that predicted by the theory, and may also reflect protein-induced perturbations in membrane viscosity.

1. INTRODUCTION

Biological membranes behave in many ways like two-dimensional fluids. For example, the organizational and phase characteristics of the membrane mimic those of simple multicomponent liquids (Aloia, 1983, 1985; Shinitzky, 1984). Moreover, many dynamic processes that take place in the membrane also have an analogue in simple fluid systems, the most obvious example being the diffusion of membrane protein and lipid (Axelrod, 1983; Petersen, 1984; McCloskey and Poo, 1984; Beck, 1987; Edidin, 1987). Much of this behavior can be understood by invoking a fluid mosaic model of membrane structure (Singer and Nicolson, 1972).

Here we are interested in understanding some of the factors that influence the lateral motion of protein molecules in a fluid bilayer; some aspects of this subject were the focus of recent reviews by Kell (1984), Gumbiner and Louvard (1985), and Jacobson et al. (1987). In many cases, mobility is under some form of biological control external to the membrane. Protein motion, for example, may be inhibited or confined to domains by interactions with peripheral structures such as tight junctions or the cytoskeletal or extracellular matrices. Energy-dependent processes such as membrane flow can lead to the large-scale redistribution of membrane components (Bretscher, 1988). In other instances, protein motion is influenced primarily by the intrinsic properties of the protein molecules themselves and of the lipid solvent. For example, it is known that stereospecific interactions can induce the formation of large, less mobile, protein aggregates. Perhaps more interestingly, we have recently come to appreciate that nonspecific interprotein interactions can also profoundly influence the diffusive motion of membrane proteins.

Here, we analyze, in detail, the diffusion of nonspecifically interacting protein molecules in the absence of external biological constraints. The diffusion of protein molecules in noninteracting (i.e., infinitely dilute) systems has already been analyzed within the confines of hydrodynamic fluid theory (Saffman and Delbrück, 1975; Saffman, 1976; Wiegel, 1980; Hughes et al., 1981); this seminal work has helped to establish the relationship between viscosity, temperature, geometry, and the bare two-dimensional diffusion coefficient, D_0, of an isolated protein in a membrane. The hydrodynamic models have

been shown to provide a good description of protein diffusion in bilayer systems that have a low concentration of protein (Vaz et al., 1984; Clegg and Vaz, 1985). However, as the concentration of protein increases the experimental diffusion coefficient for integral membrane proteins becomes density dependent and diverges from the bare value (Peters and Cherry, 1982; Tank et al., 1982; Vaz et al., 1984). Similar observations have also been made in studies of antibody molecules bound to lipid haptens at the surface of the membrane (Subramaniam et al., 1986; Tamm, 1988; Wright et al., 1988).

The concentration dependence of diffusion coefficients is in part a consequence of interactions between the protein molecules. The diffusion coefficient becomes density dependent in interacting systems because the interparticle forces are functions of interparticle separations, and the latter, of course, vary with concentration. Both direct and hydrodynamic interactions influence diffusion. Direct interactions may, for example, be hard core or electrostatic in origin, while hydrodynamic interactions reflect the protein-induced perturbation of solvent flow. In addition, membrane proteins can also perturb bilayer viscosity, and this effect can also give rise to a concentration dependence to the diffusion coefficient.

Here we focus exclusively on the effects that interactions have on self diffusion in a uniform system. The self-diffusion coefficient D^s describes the mean-squared displacement of a single protein molecule in the time t according to the equation $\langle r^2 \rangle = 4D^s(t)t$. D^s can be contrasted with the mutual-diffusion coefficient D^m, which describes the relaxation of fluctuations or gradients in concentration. D^m may be defined mathematically by Fick's Laws, which relate, for example, the particle flux $\mathbf{J}$ to the concentration gradient ∇c according to $\mathbf{J} = -D^m \nabla c$. Self- and mutual-diffusion coefficients will in general differ in interacting systems. More complete discussions of this point and its consequences for membrane systems may be found in Scalettar et al. (1988).

The effect that direct interactions have on the self-diffusion coefficient of membrane proteins has been inferred from Monte-Carlo simulations of lattice diffusion (Pink, 1985; Pink et al., 1986; Saxton, 1987*a*; Donaldson and Webb, 1988). Here we will examine the interaction dependence of self diffusion from a very different and, therefore, complementary perspective. In the spirit of the fluid mosaic model, we describe the membrane as a two-dimensional, equilibrated fluid consisting of lipid and a single species of protein. Many static (organizational) properties of the membrane can then be deduced from the theory of simple liquids, which relates molecular distributions to interparticle interactions. (Elementary discussions of fluid theory may be found in Hill [1956] and McQuarrie [1976].) Applications of fluid theory to the study of the short-ranged organization of membranes, based on protein distributions revealed in freeze-fracture electron micrographs, were recently reviewed by Abney and Owicki (1985).

Here we show that dynamic (diffusive) properties of the membrane can also be deduced from the theory of fluids. Our approach is an adaptation of theories that are widely exploited in analyses of the interaction dependence of the three-dimensional diffusion coefficient (Faraday Division, 1983; Pusey and Tough, 1985; Faraday Division, 1987). Both direct and hydrodynamic forces can be incorporated into the model. However, here we have neglected hydrodynamic effects because an appropriate form for the interaction is lacking. Our data are then ideally suited to comparison with that obtained from lattice Monte-Carlo work because the latter results inevitably contain no information about perturbation of solvent flow. We review what diffusion studies have revealed about the importance of the hydrodynamic interaction in three dimensions in the Discussion.

The paper may be outlined as follows. In the Theory section, we begin with an N-particle diffusion equation that describes a system of interacting Brownian particles and develop (after Ohtuski [1982]) a formalism for determining a time-dependent self-diffusion coefficient for membrane proteins. The theoretical equations show that to calculate a diffusion coefficient we require the interparticle force and the equilibrium distribution functions describing protein order. Under Methods we show that this information can be obtained either from continuum Monte-Carlo simulations of equilibrium particle configurations or from freeze-fracture electron micrographs that reveal protein positions. The solution of the theoretical equations is also described. In the Results section, we present our findings for a variety of simulated two-dimensional samples and for a real system of proteins from mouse liver gap junction. Finally, in the Discussion section we compare our results with the lattice Monte-Carlo and experimental data and analyze, in some detail, the factors that dictate the mobility of membrane proteins.

2. THEORY

At equilibrium, the state of a fluid may be characterized by the temperature, T, the protein lateral number density, ρ, and a pairwise-additive interprotein potential, $u(r)$. Protein order may then be described using two- and three-particle distribution functions which we call, following standard notation, $g(r)$ and $g^{(3)}(r, s, q)$, respectively. Here r, s, and q are, in order, the magnitudes of the vectors connecting particles labeled 1 and 2, and 1 and 3, and 2 and 3, respectively (see Fig. 1). Recall that the radial distribution function, $g(r)$, defines the relative

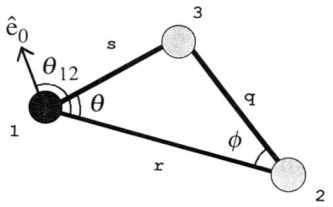

FIGURE 1 The coordinate system used in the derivation of the self-diffusion coefficient. The unit vector $\hat{e}_0$ denotes the direction of the applied oscillatory force.

probability of finding a second protein at a distance r from a given central protein, while $g^{(3)}(r, s, q)$ describes a three-particle arrangement depicted in Fig. 1. Both distributions are functions of density and are discussed extensively in the context of membrane systems in Braun et al. (1987) and Abney et al. (1987).

The kinetic formalism allows us to relate a time and interaction dependent self-diffusion coefficient, $D^s(t)$, to these equilibrium properties. We assume that self diffusion at infinite dilution is described by a given bare-diffusion coefficient, D_0, and then proceed to determine the way in which interactions modulate rates of diffusion as the density of protein increases. Our analysis will parallel the discussion in Ohtsuki (1982). Here, however, a theory and data applicable to two-dimensional diffusion are presented. Moreover, in this treatment the true equilibrium three-particle protein distribution function $g^{(3)}(r, s, q)$ is retained in the equations; in the three-dimensional theory $g^{(3)}(r, s, q)$ is approximated as a product of two-particle distribution functions as stipulated by the superposition approximation (Hill, 1956; McQuarrie, 1976).

We would like to emphasize that here we are simply computing the interaction-dependent change in the two-dimensional self-diffusion coefficient. This is an important point because it is well known that the equations that are used in *de novo* calculations of D_0 can exhibit anomalous behavior when the system is truly two dimensional. One way to circumvent this problem is simply to take into account the viscosity of the medium bounding the membrane (Saffman and Delbrück, 1975; Hughes et al., 1981). However, the formalism that we use here does not suffer from these two-dimensional anomalies, and we can therefore proceed with a strict two-dimensional analysis of the interaction dependence of D^s.

The analysis proceeds as follows. Brownian, frictional, and interprotein forces act on all proteins in the membrane. In addition, imagine that one protein in the system, designated 1, moves under the influence of an external force of the form $F_0\hat{e}_0 \exp(i\omega t)$. The motion of this special molecule can be characterized by computing a mobility, $\mu(\omega)$, defined by

$$\langle \mathbf{v}_1 \rangle = \mu(\omega) F_0 \hat{e}_0 e^{i\omega t}. \tag{1}$$

Here $\langle \mathbf{v}_1 \rangle$ is the average velocity of protein 1. A frequency-dependent diffusion coefficient, $\tilde{D}^s(\omega)$, for protein 1 is then simply related to the mobility according to the equation

$$\tilde{D}^s(\omega) = k_B T \mu(\omega). \tag{2}$$

The mobility defined in Eq. 1 is an important quantity because the motion of protein molecules that are moving under the influence of only the real forces; Brownian, frictional, and interprotein can be deduced once $\mu(\omega)$ is known. Specifically the usual time-independent, long-ranged self-diffusion coefficient, $D^s(t = \infty)$, of such a protein is determined by $\mu(\omega)$ in the limit that $\omega \rightarrow 0$ (Kubo, 1966)

$$D^s(t = \infty) = \lim_{\omega \to 0} k_B T \mu(\omega) = \lim_{\omega \to 0} \tilde{D}^s(\omega). \tag{3}$$

Moreover, it will be shown later that the temporal (or short-ranged) behavior of the diffusion coefficient can be determined if $\tilde{D}^s(\omega)$ is known for nonzero values of the frequency.

To calculate $\mu(\omega)$ we require an expression for $\langle \mathbf{v}_1 \rangle$. The average velocity of a particle may be computed from its equation of motion; an appropriate such equation for protein 1 is a Langevin equation of the form

$$m \frac{d\mathbf{v}_1}{dt} = -f^s \mathbf{v}_1 + F_0 \hat{e}_0 e^{i\omega t} - \sum_{j>1} \nabla_1 u(r_{j1}) + F_{\text{Brown}}(t). \tag{4}$$

In this equation, m is the mass of a protein molecule, f^s is the friction coefficient, ∇_1 is the usual gradient operator acting only on the coordinates of particle 1, r_{j1} is the magnitude of the vector $\mathbf{r}_{j1} = \mathbf{r}_j - \mathbf{r}_1$ connecting the positions of particles j ($\mathbf{r}_j$) and 1 ($\mathbf{r}_1$), and $F_{\text{Brown}}(t)$ is a random Brownian force. An expression for $\langle \mathbf{v}_1 \rangle$ can be obtained by averaging Eq. 4:

$$\langle \mathbf{v}_1 \rangle = \frac{1}{f^s}\left[F_0 \hat{e}_0 e^{i\omega t} - \frac{1}{\rho}\int \nabla_1 u(r) P_2(\mathbf{r}, t) d\mathbf{r}\right]. \tag{5}$$

Here $\mathbf{r} = \mathbf{r}_2 - \mathbf{r}_1$, and $P_2(\mathbf{r}, t)$ is a two-particle distribution function whose time dependence derives from the application of the time-dependent external force. In obtaining Eq. 5, the inertial term $m(d\mathbf{v}_1/dt)$ was neglected, the positional independence of the applied force was invoked, the term involving the interaction potentials was averaged by integration over the appropriate distribution function, and the Brownian term was averaged to zero (by definition). Inertial terms relax with a characteristic time on the order of m/f^s (Rallison and Hinch, 1986); therefore, for most membrane proteins the neglect of inertial terms is justified for times that exceed $\sim 10^{-13}$ s.

From Eq. 5 it can be seen that to determine $\langle \mathbf{v}_1 \rangle$ an expression for $P_2(\mathbf{r}, t)$ is required. It is certainly reasonable to postulate that $P_2(\mathbf{r}, t)$ is closely related to (i.e., perturbed about) the equilibrium two-particle distribution function, $g(r)$. In Appendix A we develop this idea rigorously and show that if we introduce a complex radial perturbation function, $p(r, \omega, \rho)$, relating $P_2(\mathbf{r}, t)$ and $g(r)$, it will satisfy an integrodifferential equation of the form

$$r^2 g \frac{d^2p}{dr^2} + \left(r^2 \frac{dg}{dr} + rg\right)\frac{dp}{dr} - gp + \frac{\rho\beta r}{2}\int_0^\infty F(r, s)p(s, \omega, \rho)\, ds - i\frac{\omega}{2D_0} gpr^2 = -r^2 \frac{dg}{dr}, \quad (6a)$$

where we have utilized the abbreviations

$$F(r, s) = \frac{d}{dr}[rA(r, s)] - B(r, s), \quad (6b)$$

$$A(r, s) = \int_0^{2\pi}\left\{\frac{du}{ds}\cos\theta + \frac{du}{dq}\cos\phi\right\} \cdot \cos\theta g^{(3)}(r, s, q)sd\theta, \quad (6c)$$

$$B(r, s) = \int_0^{2\pi}\left\{\frac{du}{ds} - \frac{s}{q}\frac{du}{dq}\right\}\sin^2\theta g^{(3)}(r, s, q)sd\theta. \quad (6d)$$

Here $\cos\theta = (r^2 + s^2 - q^2)/2rs$ and $\cos\phi = (r^2 + q^2 - s^2)/2rq$ (see Fig. 1). Details of the solution of this equation for the complex $p(r, \omega, \rho)$ are given in Section 3.3. Note also that we will henceforth suppress display of the ρ (and occasionally the ω) dependence of $p(r, \omega, \rho)$.

The appropriate boundary conditions to impose on $p(r, \omega)$ state that the radial perturbation approaches zero as r becomes very large,

$$\lim_{r\to\infty} p(r, \omega) = 0, \quad (7a)$$

and that the flux, $\mathbf{J}$, (see Eq. A2b in Appendix A) vanishes when two particles collide,

$$g\frac{dp}{dr} + \frac{\rho\beta}{2}\int_0^\infty A(r, s)p(s, \omega)ds = -g. \quad (7b)$$

Eq. 7b is evaluated at a specific value of r that reflects contact.

Once $p(r, \omega)$ is calculated from Eqs. 6 and 7, the full time-dependent distribution function $P_2(\mathbf{r}, t)$ is known (see Appendix A). Hence, $\langle \mathbf{v}_1 \rangle$ may be determined from Eq. 5, and the frequency-dependent mobility and diffusion coefficient found using Eqs. 1 and 2, respectively. It follows that

$$\frac{\tilde{D}^s(\rho, \omega)}{D_0} = 1 - \Delta\tilde{D}^s(\omega), \quad (8a)$$

where

$$\Delta\tilde{D}^s(\omega) = -\frac{\rho\beta\pi}{2}\int_0^\infty \frac{du}{dr} p(r, \omega)g(r, \rho)rdr. \quad (8b)$$

The usual long-time self-diffusion coefficient is obtained in the $\omega \to 0$ limit, as indicated in Eq. 3.

The temporal variation of the diffusion coefficient can also be extracted from this formalism. First the velocity autocorrelation function, $C(\tau)$, is calculated as the Fourier transform of $\tilde{D}^s(\rho, \omega)$:

$$C(\tau) = \frac{4}{\pi}\int_0^\infty Re[\tilde{D}^s(\rho, \omega)]\cos\omega\tau d\omega. \quad (9)$$

Second, the velocity autocorrelation function is used to calculate the mean-squared displacement of a diffusing molecule through the standard relationship

$$\langle [\mathbf{r}(t) - \mathbf{r}_0]^2 \rangle = 2\int_0^t (t - \tau)C(\tau)d\tau = 4D_0 t\left[1 - \int_0^t (1 - \frac{\tau}{t})\Delta C(\tau)d\tau\right]. \quad (10)$$

In Eq. 10, $\Delta C(\tau)$ is simply the Fourier transform of $\Delta\tilde{D}^s(\omega)$, defined by analogy with Eq. 9. Finally, a time-dependent diffusion coefficient can be found from the mean-squared displacement:

$$D^s(t) = \frac{\langle [\mathbf{r}(t) - \mathbf{r}_0]^2 \rangle}{4t}. \quad (11)$$

We close out this theoretical section with a brief discussion of self diffusion in dilute interacting systems; this subject is treated more completely in Scalettar et al. (1988). The mathematical description simplifies considerably in the dilute limit because the probability of finding three particles in proximity is low. The three-particle distribution function and the associated integrals, 6c and 6d, can, therefore, be thrown out of the theory and expression 6 rewritten as purely a differential equation for the perturbation function. Moreover, for a dilute solution $g(r)$ follows the analytical relationship $g(r) = \exp[-\beta u(r)]$. Hence in a dilute fluid we find that the diffusion coefficient will vary linearly with ρ as follows:

$$\frac{D^s\rho}{D_0} = 1 + \frac{\rho\beta\pi}{2}\int_0^\infty \frac{du}{dr} p(r)e^{-\beta u(r)} rdr. \quad (12)$$

3. MATERIALS AND METHODS

Here, we will describe, in order, (*a*) our sources of data, (*b*) the determination of particle distribution functions and the kernel $F(r, s)$, (*c*) the solution of Eqs. 6 and 7 for $p(r)$, and, (*d*) the use of $p(r)$ to find D^s/D_0.

3.1. Sources of data

Data were obtained from two sources: Monte-Carlo generated configurations of particles interacting through specified analytical potentials and freeze-fracture electron micrographs that reveal the positions of real proteins in bilayer membranes.

3.1.1. Analytical potentials

Analytical potentials were chosen to model the effects of both repulsive and attractive interactions on the self-diffusion coefficient.

The simplest interaction we analyzed is the excluded-volume repulsion (known also as the hard-core or the hard-disk interaction):

$$u_{HC}(r) = \begin{cases} \infty & r \le d_{HC} \\ 0 & r > d_{HC}. \end{cases} \tag{13}$$

Such a potential describes the interaction between two particles with hard-core diameters d_{HC}. See Fig. 2 A. The associated force is a delta function centered on $r = d_{HC}$.

It is probable that protein molecules are not entirely rigid, and that, therefore, a softer potential might better model their interaction at small separations. It is also possible that the proteins may induce structural changes in the bilayer that give rise to longer-ranged, attractive, lipid-mediated interactions between proteins (Abney and Owicki, 1985). The interplay between softer repulsions and long-ranged attractions was modeled with a 6-4 potential, defined as

$$u_{64}(r) \equiv \frac{27}{4}\epsilon[(\sigma/r)^6 - (\sigma/r)^4]. \tag{14}$$

This potential crosses zero at $r = \sigma$ and attains a maximum depth of ϵ at $r = r_0 = (3/2)^{1/2}\sigma$. See Fig. 2 *A*. The 6-4 pair force, found by differentiation, is repulsive for $r < r_0$ and attractive for $r > r_0$.

For computational economy, a fluid with repulsions and attractions (fluid A) was simulated by truncating the 6-4 potential at $r = 2.5\, r_0 = 3.0619\sigma$ and shifting it up slightly (by $u_{64}(2.5\, r_0) \approx 0.07\epsilon$) to maintain continuity. The actual potential studied was

$$u_A(r) = \begin{cases} u_{64}(r) - u_{64}(2.5\, r_0) & r < 2.5 r_0 \\ 0 & r \ge 2.5 r_0. \end{cases} \tag{15}$$

The force is unaltered by the truncation, except that it is identically zero for $r \ge 2.5\, r_0$.

To isolate the role that attractions play in determining the diffusive behavior of fluid A, a purely repulsive fluid (fluid R) was simulated with a potential created by subtracting from the 6-4 potential its minimum value, $u_{64}(r_0) = -\epsilon$, and setting the potential equal to zero beyond $r = r_0 = 1.2247\sigma$:

$$u_R = \begin{cases} u_{64}(r) - u_{64}(r_0) & r < r_0 \\ 0 & r \ge r_0. \end{cases} \tag{16}$$

This Weeks-Chandler-Andersen decomposition (Chandler et al., 1983) preserves precisely the repulsive component of the 6-4 force. The force is zero in the attractive domain of the 6-4 potential, i.e., for $r \ge r_0$.

3.1.2. Gap-junction potentials

Interprotein forces and potentials describing the interaction between proteins in mouse liver gap junction were obtained from freeze-fracture electron micrographs as described previously (Braun et al., 1984; Abney et al., 1987). This system was assumed to contain a single species of protein in a fluid membrane. We present results based on potentials derived from two junctions, denoted 1 and 2 in Abney et al. (1987). The average interparticle separation in both systems was ~10 nm. Both potentials are repulsive at all separations and are significant relative to thermal particle energies (i.e., $u[r]/k_BT \gtrsim 1$) for separations $\lesssim$12 nm. See Fig. 2 *B*.

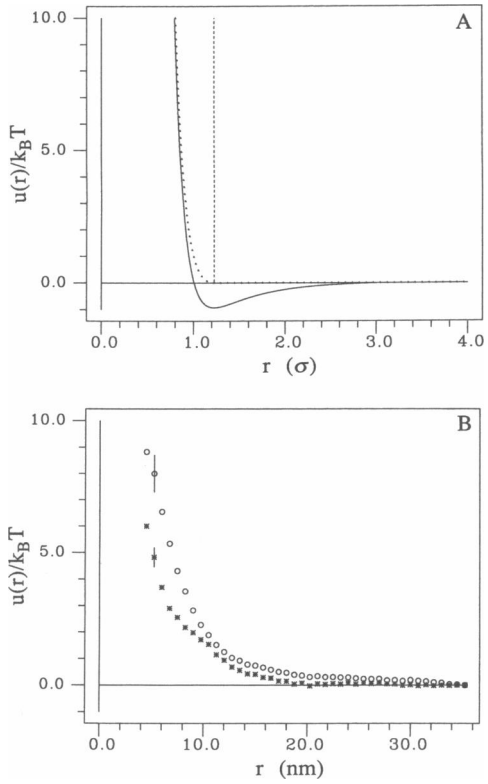

FIGURE 2 Potentials used in the calculation of diffusion coefficients. Panel A shows the analytical potentials: hard core (– – –), fluid A (——), and fluid R (· · · · ·). The hard-core diameter d_{HC} associated with the excluded-volume interaction is arbitrarily shown equal to r_0; only the product $\pi\rho d_{HC}^2/4 \equiv f_A$ determines the rate of change of the diffusion coefficient. Panel B shows the gap-junction potentials: junction 1 (O) and junction 2 (*). The vertical bars show the largest absolute uncertainty associated with a single value in each potential.

3.2. Computation of distribution functions and kernel $F(r, s)$

Distribution functions were computed from particle coordinates according to algorithms described in Abney (1987) and Braun et al. (1987). The computation of other configuration-derived functions, e.g., $A(r, s)$ and $B(r, s)$, proceeded similarly. To reduce noise arising from the finite size of the sample particle configurations, both sets of functions were tabulated over bins of finite width Δ (typically 2.5% to 7.5% of the average interparticle spacing). For example, bin-averaged values of $g(r)$ were reported as $\langle g(r_i)\rangle$ at the discrete points $\{r_i\}$. It was assumed that, because the bins were small, these averaged values were excellent approximations to the true values. For example, we took $\langle g(r_i)\rangle \approx g(r_i)$. Subsequent numerical analysis based on these functions (Sections 3.3 and 3.4) made use of this same binning. Data were collected for 80–200

bins; the choice of lower and upper cutoffs was made before analysis began.

Details of the computations depended on the source of data. However, once $A(r, s)$ and $B(r, s)$ were known, the function $F(r, s)$, defined in Eq. 6b, was computed numerically independent of source. The derivative was evaluated based on a five-point quartic fit (Savitzky and Golay, 1964). We consider the source-dependent computations below.

3.2.1. Computations based on analytical potentials

Simulated equilibrium particle configurations, corresponding to the analytical potentials, were generated for 256 particles in a square patch using the standard Metropolis et al. (1953) Monte-Carlo algorithm; a detailed discussion of our simulation procedure was given in Braun et al. (1987). Particle positions were perturbed sequentially, with one cycle defined as one attempted movement of every particle in the system. Simulations were begun with the particles in a crystalline array; typically several thousand cycles were run to ensure equilibration before data were taken. The functions $g(r)$, $A(r, s)$, and $B(r, s)$ were then computed by averaging over particle positions during the course of the simulation. This averaging was performed every ten or so cycles for a total of 2,000 to 5,000 cycles to achieve a good signal-to-noise ratio.

Analysis of the simulated hard-disk fluid required special consideration because of the unique properties of the delta-function force. The Monte-Carlo algorithm was simplified: trial moves that gave rise to overlaps were rejected, those that did not were accepted. As is evident upon visual inspection of Eqs. 6 and 7b, contributions to $A(r, s)$ and $B(r, s)$ arose only for q or s at contact. These functions are well-approximated by using values averaged over the smallest bin, i.e., for $d_{HC} < s < d_{HC} + \Delta$ and $d_{HC} < q < d_{HC} + \Delta$.

In the dilute limit, simulations were not necessary. The radial distribution function is given analytically, i.e., $g(r) = \exp[-\beta u(r)]$. Since three-particle interactions may be neglected, $F(r, s) = 0$. To facilitate use of numerical techniques described below, we still reported values of $g(r)$ at the midpoints of discrete bins: $g(r_i)$.

3.2.2. Computations based on gap-junction potentials

The freeze-fracture data required somewhat different analysis. Here the interparticle force was not known initially, but was computed from protein coordinates revealed in the micrographs. Specifically, the interprotein force is defined in terms of the two- and three-particle distribution functions according to the equilibrium Born-Green-Yvon (BGY) equation (see Braun et al., 1987). If these distribution functions are determined from particle coordinates, the BGY equation may be inverted and the interprotein force (corresponding to the native, or observed, density) calculated. This procedure was followed to determine the gap-junction potentials shown in Fig. 2 *B* and is described in Abney et al. (1987).

Particle coordinates were then analyzed a second time, and, together with the BGY force, the coordinate information was used to determine $A(r, s)$ and $B(r, s)$. Results corresponding to non-native densities could, in principle, have been calculated from a Monte-Carlo simulation using the BGY-derived potential; however, if the true potential varies with concentration (Pearson et al., 1984; Abney and Owicki, 1985) such an extension to unobserved densities would be invalid.

3.3 Solution of perturbation equations for $p(r, \omega)$

The perturbation $p(r, \omega)$ was obtained as the solution of Eq. 6 subject to the boundary conditions in Eq. 7, once $g(r)$ and $F(r, s)$ had been computed. We expressed the intrinsically complex $p(r, \omega)$ as the sum of real (p_r) and imaginary (p_i) components

$$p(r, \omega) = p_r(r, \omega) + ip_i(r, \omega). \tag{17}$$

Collecting real and imaginary terms separated Eq. 6 into two coupled, integrodifferential equations. After the procedure outlined in Appendix B, we converted these equations into a system of discrete linear equations, i.e., a matrix equation.

The solution to the matrix problem was obtained using LINPACK subroutines SGECO and SGESL (Dongarra et al., 1979). These subroutines are based on an algorithm which utilizes Gaussian elimination with partial pivoting (Forsythe et al., 1977). The matrix problem itself is well conditioned: the relative variations in the (input) distribution functions and (output) perturbation function were of the same order of magnitude for different data sets that corresponded to identical conditions. The stability and accuracy of the method are manifest in the size of our error bars (see Section 4) and in the success of our hard-disk control experiments (see Section 5.1).

In the dilute limit we used the same formalism; however, there was no contribution from $F(r, s)$. In the special case of excluded-volume interactions, the perturbation $p(r, \omega = 0)$ was found analytically (Scalettar et al., 1988).

3.4. Determination of diffusion coefficients

To complete the calculation of diffusion coefficients, the real component of $\Delta\tilde{D}^s(\omega)$ must be known. This quantity was computed from the real component of $p(r, \omega)$. For the long-ranged analytical and gap-junction potentials, the integral in Eq. 8b was evaluated from discrete values of the requisite functions using Simpson's Rule (Bevington, 1969). For the hard-core potential, the only contribution to the integral came at contact. In the latter case, $p_r(d_{HC}, \omega)$ and $g(d_{HC})$ were obtained by extrapolating $p_r(r, \omega)$ and $g(r)$ back to contact separation, d_{HC}. This was done using a two-point linear fit based on the values of these functions in the two smallest bins $> d_{HC}$.

The usual long-ranged diffusion coefficient was determined directly from Eq. 8a according to its definition, $D^s(t = \infty)/D_0 = 1 - \Delta\tilde{D}^s(\omega = 0)$. Only long-ranged diffusion coefficients were calculated in the dilute case.

The computation of a time (or distance) dependent diffusion coefficient was more involved (Eqs. 8–11) but was found by us to be considerably simplified by following the procedure outlined below. $\Delta\tilde{D}^s(\omega)$ was computed at ~30 logarithmically-spaced values of ω between 0 and 200. These values were then accurately fit to a weighted sum of three simple, decaying exponential functions; no physical significance was attributed to the best-fit parameters. The Fourier transform that appears in Eq. 9 for the velocity autocorrelation function was then performed analytically. Once $\Delta C(\tau)$ was known it was substituted into Eq. 10 for the mean-squared displacement; division by $4D_0t$ then gave an analytical expression for $D^s(t)/D_0$ in terms of the fitting parameters. The magnitude of D_0 is reflected in the values of t; a change from $D_0^{(i)}$ to $D_0^{(f)}$ scales the time according to $t^{(f)} = [D_0^{(f)}/D_0^{(i)}]t^{(i)}$.

By calculating both the diffusion coefficient and the mean-squared displacement corresponding to a given time, the spatial dependence of the diffusion coefficient, $D^s(r)/D_0$, was determined. There are two principal reasons for focusing on the spatial, rather than the temporal, decay of D^s/D_0. First, the spatial dependence of the diffusion coefficient is independent of D_0, while the time dependence is not. Second, it seems most natural to interpret the decay of the diffusion coefficient in terms of the number of neighbor encounters; this can easily be done by following the spatial variation in D_s, if the average interparticle spacing is taken as the unit of distance.

4. RESULTS

We present results for the hard-disk potential, the 6-4 potentials (fluid A and fluid R), and the gap-junction potentials (junction 1 and junction 2) at the in vivo densities.

The results are displayed graphically, in two basic forms. The long-ranged diffusion coefficient $D^s(t = \infty)/D_0$ is plotted as a function of density, and the short-ranged diffusion coefficient $D^s(r)/D_0$ is plotted as a function of displacement (for multiple densities).

The particle density appearing in the theoretical equations is simply the number of particles per unit area (i.e., the number density). However, when our numerical results are displayed in graphical form and compared with the lattice and experimental work, a different set of units will sometimes be used. For the hard-core and gap-junction interactions, D^s/D_0 is given as a function of area fraction $f_A \equiv \pi\rho d_{HC}^2/4$ of protein coverage. For the 6-4 potentials, a unique area fraction cannot be assigned; the standard unit of concentration is the reduced density ρ^* defined by $\rho^* \equiv \rho\sigma^2$, where σ is given in Eq. 14.

4.1. Long-ranged excluded-volume results

A hard-disk fluid was simulated at two area fractions: $f_A = 0.25$ and 0.50. We chose $d_{HC} = 1$, $\Delta = 0.02$, and an upper cutoff of $r = 5d_{HC}$. There were thus 200 bins. Samples were initially equilibrated for 2,500 cycles. To assess the noise sensitivity of the computations, we ran two 5,000-cycle simulations at each density; averages were calculated every ten cycles of the run. An estimate of the uncertainty was then obtained by averaging the diffusion coefficients derived from the two data sets at each density. Results are plotted in Fig. 3.

In the dilute limit the diffusion coefficient obeys the relationship

$$D^s_{HC}(f_A)/D_0 = 1 - 2f_A. \tag{18}$$

This function is also displayed in Fig. 3. The results obtained from the general and dilute theories are in close agreement for small area fractions, but diverge as f_A increases. Note that the dilute expression always overestimates the reduction in D^s/D_0.

4.2. Long-ranged 6-4 results

In our analysis of the 6-4 potentials, we set $\epsilon = k_BT$, which renders the depth of the attractive well in fluid A equal to one k_BT.

Fluid A and fluid R were simulated at six reduced densities: $\rho^* = 0.1$ and 0.2 (1 run each, 2,500 cycles) and $\rho^* = 0.3$, 0.5, 0.7, and 0.8 (2 runs each, 2,000 cycles). We chose $\Delta = 0.05$ and an upper cutoff of $r = 4\sigma$. The precise number of bins depended on the smallest bin for which $g(r) \neq 0$. Configurations were initially equilibrated for 2,000 cycles. Data collection and error analysis were conducted as described above. Radial distribution functions for these fluids at $\rho^* = 0.0$, 0.3, and 0.8 are plotted in Fig. 4. The diffusion results are plotted in Fig. 5.

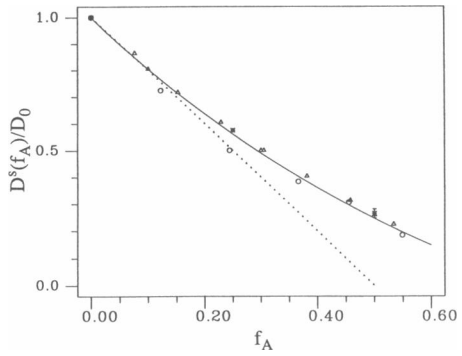

FIGURE 3 Comparison of the long-ranged self-diffusion coefficients for the excluded-volume interaction with the hard-hexagon data of Pink (1985) and Saxton (1987*a*). Our results (*) were obtained as described in the text and are plotted with error bars. Pink's results (O) were taken from Table I and Fig. 2 in his paper. Saxton's results (Δ) for his $r = 4$ proteins on the hexagonal lattice (Fig. 5 of his paper) were obtained from the author (personal communication). The (*solid*) curve is drawn using Eq. 20, which fit Saxton's data to within ±5%. The (*dotted*) line represents the dilute expression given in Eq. 18; it is continued to higher densities as a reference.

The diffusion data should be contrasted with the predictions of the dilute theory:

$$D^s_A(\rho^*)/D_0 = 1 - 1.68\rho^* \quad \text{Fluid A} \tag{19a}$$

$$D^s_R(\rho^*)/D_0 = 1 - 1.48\rho^* \quad \text{Fluid R.} \tag{19b}$$

The linear relationships 19a and 19b are also shown in Fig. 5. As was the case with the excluded-volume interactions, the dilute theory agrees with the more general formalism for small (reduced) densities, but underestimates D^s/D_0 as ρ^* increases.

4.3. Long-ranged gap-junction results

The diffusion coefficient, $D^s(\rho_{native})$, for proteins in the murine liver gap junction was computed for both junction 1 and junction 2. Each junction was analyzed (i.e., particle coordinates were tabulated, distribution functions computed, etc.) over two nonoverlapping regions, as in Abney et al. (1987). An estimate of the error in $D^s(\rho_{native})$ was obtained by averaging the diffusion results from the two sub-regions; data from different junctions

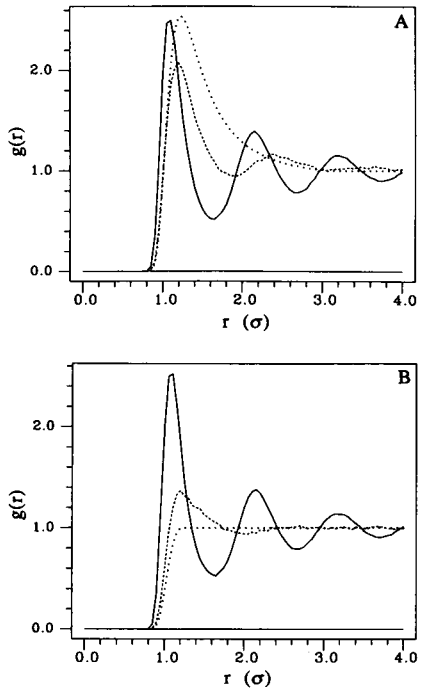

FIGURE 4 Density dependence of the radial distribution functions for fluids A and R. Panel A shows $g(r)$ for fluid A at $\rho^* = 0.0$ (· · · · ·), 0.3 (– – –), and 0.8 (——). Panel B shows these functions for fluid R, using the same notation. For $\rho^* = 0.0$, $g(r)$ was computed analytically from the relationship $g(r) = \exp[-\beta u(r)]$. For $\rho^* = 0.3$ and 0.8, values were obtained as averages computed during Monte-Carlo simulations as described in the text. We estimate the errors to be ~1%. The radial distribution function gives a measure of the order in the fluid as a function of radial distance r. Order is lowest for $\rho^* = 0.0$. As the density of the system is raised, order increases and coordination shells, corresponding to regions of enhanced ($g > 1$) and diminished ($g < 1$) occupancy, develop; the average center-to-center distance, given by the location of the first peak in $g(r)$, decreases. At the two lowest densities, particles are significantly closer in fluid A, brought together by attractive interactions. By $\rho^* = 0.8$, the identical repulsions dominate the structure of both fluids, and the two distribution functions are virtually superimposable.

were analyzed separately. We find $D^s_{(1)}/D_0 = 0.435 \pm 0.036$ and $D^s_{(2)}/D_0 = 0.614 \pm 0.040$. The gap-junction data were not extrapolated to infinite dilution because the computed pair potential may not be valid at non-native densities (see Section 3.2.2).

4.4. Spatial dependence of diffusion coefficients

The spatial (or temporal) dependence of the self-diffusion coefficient was computed for each potential, at each density analyzed above, by following the procedure outlined in Section 3.4. In all cases the diffusion coefficient decayed rapidly (within one or two times the average

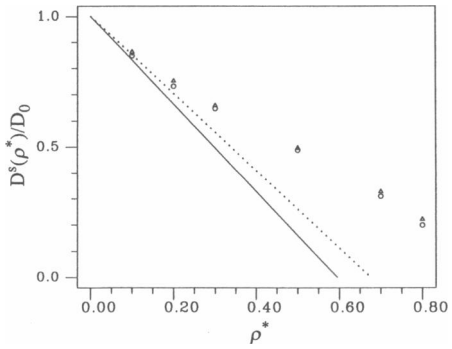

FIGURE 5 Long-ranged self-diffusion coefficients for fluids A and R. Values were obtained as described in the text and are plotted as points for fluid A (○) and fluid R (△). Relative errors in the average diffusion coefficient were less than 4.5% (i.e., always less than the size of the symbols). The straight lines represent the extrapolation of the low density results for A (——) and R (· · · · ·) as given in Eqs. 19*a* and *b*. The dilute results are strictly valid only for small densities, but have been drawn to higher densities as a reference.

interparticle separation) to its steady-state, long-ranged value. When two simulations were run at the same density, the associated spatial dependences were identical (within the error bars in the long-ranged diffusion coefficients). Representative spatial decays are displayed for the 6-4 potential at $\rho^* = 0.3$ and 0.8 in Fig. 6.

5. DISCUSSION

5.1. Analysis of long-ranged excluded-volume results

To date, theoretical analyses of interaction-dependent protein diffusion have focused primarily on systems that

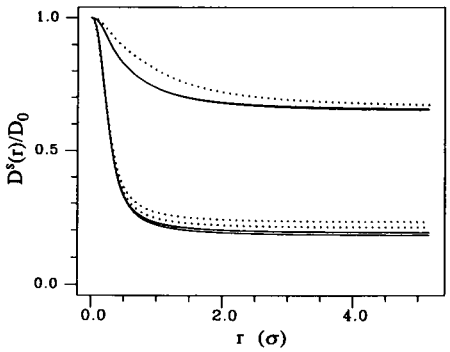

FIGURE 6 Spatial dependence of the self-diffusion coefficients for fluids A and R. We give results for A (——) and R (· · · · ·) at $\rho^* = 0.3$ (*upper curves*) and 0.8 (*lower curves*). Eight curves are shown, two for each density and potential; associated plots overlap when the error is sufficiently small. Radial distribution functions for these two fluids at these densities are given in Fig. 4.

interact through excluded volume (Pink, 1985; Saxton, 1987a). In these studies, Monte-Carlo methods were used to move hexagonally shaped proteins on a lattice. By associating a time interval with each step, the authors were able to compute diffusion coefficients.

The results obtained by both Pink (1985) and Saxton (1987a) are in close quantitative agreement with each other (see Fig. 3) and were summarized in a polynomial form by Saxton (his Eq. 12):

$$D^s(f_A)/D_0 = 1 - 2.1187f_A + 1.8025f_A^2 - 1.6304f_A^3 + 0.9466f_A^4. \quad (20)$$

To assess the level of agreement between the continuum and lattice models, we have compared our results with the relevant hard-core data at selected area fractions; see Fig. 3. The similarity is striking. We also note that our dilute result, $D^s(f_A)/D_0 = 1 - 2f_A$, agrees with the low-density lattice Monte-Carlo data to within Saxton's error. For dilute solutions, it is only necessary to retain the linear term in Eq. 20; hence, for such systems the lattice results imply $D^s(f_A)/D_0 = 1 - 2.1187f_A$.

What is the significance of this agreement? Pink and Saxton have utilized Monte-Carlo methods to look at the effects that excluded-volume interactions have on lattice diffusion. We have described interaction-dependent continuum diffusion using a formalism taken from the theory of fluids. Each of the analyses must inevitably be somewhat approximate. Nevertheless, the consensus achieved for the excluded-volume interactions, with these rather disparate methods, indicates that both approaches correctly model the processes under consideration. We can thus view, with considerable confidence, results presented here for which no comparable data exist.

5.2. Analysis of long-ranged 6-4 results

We have obtained diffusion data for the two analytical 6-4 potentials at a variety of densities, as shown in Fig. 5. These potentials were chosen to assess the role that soft repulsions and weak, long-ranged attractions play in determining the diffusion coefficient; for this latter reason, they contain identical repulsive forces but only fluid A contains attractions. The attractions were kept weak ($\epsilon = k_BT$) to ensure that the simulations modeled single-phase fluids. The phase diagram for the 6-4 potential is not available; however, we noted that a doubling of ϵ seemed to induce a two-phase fluid for the densities we studied (data not shown).

Both interactions induce a similar monotonic reduction in the diffusion coefficient with density; this fact suggests that repulsions are the principal determinant of D^s/D_0 for these fluids. In each case, the numerical results obtained from the general formalism blend into the predictions of the dilute theory as the density of the system decreases.

In fact, the functional relationship between D^s/D_0 and ρ is also similar for the long-ranged 6-4 potentials and the excluded-volume interaction. It therefore appears that the form of the interparticle interaction may be less important than density in determining the modulation in the self-diffusion coefficient. We suggest a mechanistic rationale for this observation. As the density increases, more and closer neighbors require a diffusor to travel a more tortuous pathway through the membrane; hence the decrease in D^s/D_0 may be dictated largely by an effect that is independent of the sign of the force. We suspect that for particles of nonzero size, the effects of interactions are minimized for systems that interact only through excluded volume. Additional long-ranged repulsions effectively increase the size of the particles, further reducing the pathways available for diffusion. Attractions could effectively tether particles together, causing them to move as larger, less mobile, units. Kinetic differences created by repulsions and attractions are discussed in Section 5.4.

Why are the effects of interactions on diffusion consistently overestimated by the dilute expressions? In the dilute limit, path blockage is probably in some sense pairwise additive. However, as additional proteins are added to the system, multiparticle configurations arise in which blockage overlaps. Therefore, at high densities the combined effect is less than the pairwise sum, and so the diffusion coefficient is not reduced as much as is predicted by extrapolating the dilute theory. At sufficiently high densities, the membrane may undergo a fluid-to-solid phase transition that could profoundly reduce mobility.

There is only one other published study of the effects of attractions on self diffusion in membrane systems. Pink et al. (1986) analyze the diffusion of nearest-neighbor attractive proteins within the confines of a lattice model. Here the interactions produce protein clusters, which are modeled as immobile. In reality, such clusters should be thought of as larger particles or porous patches that diffuse at nearly the same rate as a single particle (Wiegel, 1980). In the Pink model, weak attractions produce a fewfold reduction in D^s/D_0, in qualitative agreement with our findings. Sufficiently strong attractions lead to lateral phase separation and clustering of the majority of the protein; when the clusters are viewed as immobile, the diffusion coefficient decreases substantially.

5.3. Analysis of long-ranged gap-junction results

Based on our theoretical analysis of the experimental data, we computed relative diffusion coefficients for

gap-junction proteins in junctions 1 (0.435 ± 0.036) and 2 (0.614 ± 0.040). It seems most reasonable to express these results as a function of the area fraction occupied by the protein; therefore, we need estimates of the number density and hard-core diameter of the proteins. The number density in this analysis was scaled to $9{,}330/\mu m^2$, as described in Abney et al. (1987). Estimates of the particle diameter range from 5.5 nm (based on the smallest bin for which $g(r) \neq 0$ in our work) to 7.0 nm (based on crystallographic data). The above disparity could reflect errors inherent in our analysis, or the fact that the protein is not exactly circular (see Middlehurst and Parker (1986) for a discussion of $g(r)$ for noncircular proteins). These values suggest an area fraction between 22 and 36%.

We cannot make a comparison with experimental diffusion coefficients because D^s has not been measured for gap-junction proteins. We must be content noting that we have determined the interaction-dependent contribution to the diffusion coefficient for these proteins, and that, at the in vivo area fraction, D^s/D_0 has approximately the same value in the gap-junction and model systems. There are several possible explanations for the difference in diffusion coefficients calculated from the data in junctions 1 and 2. For example, if the proteins in junction 2 were really at a lower density than those in junction 1, the smaller modulation in 2 would follow immediately. Further reasons to suspect a difference in density are discussed in Abney et al. (1987).

5.4. Analysis of the spatial dependence of diffusion coefficients

The review article by Pusey and Tough (1985) notes that the three types of forces acting on each solute particle—Brownian, interparticle, and hydrodynamic—influence the diffusive motion over a different characteristic time scale. Brownian forces are in general much stronger than interparticle interactions. Thus, at very short times, the motion of a protein is determined exclusively by its Brownian interaction with the lipid solvent; in this limit, the diffusion coefficient is given by D_0. As diffusive motion extends over longer time (or distance) scales, interparticle interactions become increasingly important. The diffusion coefficient decreases and eventually attains its long-time, steady-state value. The nature of the motion over intermediate time scales is determined by the local structure of the fluid, as embodied in the distribution functions.

We have followed the decay of the self-diffusion coefficient to its steady-state value as a function of the root-mean-squared displacement of the protein. Representative results for fluids A and R at two reduced densities are shown in Fig. 6. For each potential analyzed, the diffusion coefficient is initially equal to D_0 and essentially reaches its long-time value within a distance equal to one or two times the average interparticle separation in the system; the majority of the decay takes place within a single spacing. A similar observation was made previously for excluded-volume interactions on a lattice (Saxton, 1987b).

The detailed kinetic behavior of the diffusion coefficient is determined by the detailed structure of the fluid. In the 6-4 fluids, we see that at low densities $D^s(r)/D_0$ falls off more rapidly with distance when attractions are present; this difference between fluid A and R diminishes as the density increases. Such behavior is in accord with the fact that attractions tend to keep particles in closer proximity and thus slightly lessen the distance between interacting neighbors, particularly at low densities (see Fig. 4 in this paper and Fig. 4 in Braun et al., 1987).

The kinetic results suggest that self diffusion over distances larger than one or two times the average interparticle separation in the system is correctly described by the steady-state diffusion coefficient. Hence, physiological diffusive motions that span distances between ~10 nm and cellular dimensions proceed at a rate prescribed by $D^s(t = \infty)$. It also follows that experimental techniques that monitor self diffusion over such distances measure $D^s(t = \infty)$. Thus, $D^s(t = \infty)$ is obtained from the best known and most widely exploited method for determining self-diffusion coefficients (Phillies, 1975) in membranes, fluorescence recovery after photobleaching, or FRAP (Peters, 1981; Vaz et al., 1982; Axelrod, 1985; Petersen et al., 1986).

Only at the nearest-neighbor level is there likely to be any need for attributing a spatial (or temporal) dependence to the diffusion coefficient. Such nearest neighbor motions might play a role, for example, in bioenergetic electron transfer (Hackenbrock, 1981; McCloskey and Poo, 1984) or in signal transduction by the hormone-receptor adenylate-cyclase system (Peters, 1985). Moreover, experimental techniques (e.g., pyrene excimer formation, fluorescence energy transfer, triplet-triplet annihilation, and magnetic resonance techniques) that follow local motions can measure short-ranged diffusion coefficients; however, to date, such techniques have been used exclusively to measure the mobility of lipids. This subject is briefly reviewed by McCloskey and Poo (1984) and Edidin (1987). We also note that Eisinger et al. (1986) have presented a Milling Crowd Model that analyzes short-ranged diffusion of excimeric membrane probes in the presence of larger, protein obstacles.

Presumably, some of the short-ranged diffusion techniques could also be used to look at protein mobility. However, the protein diffusion data could be somewhat difficult to interpret; a theoretical analysis of short-

ranged protein diffusion experiments may have to include a description of rotational motion, at least for larger proteins, since the proximity of probes tethered to different proteins will depend on molecular orientation. We also note that a measured short-ranged diffusion coefficient will really represent some value that is averaged over (portions of) the decay from D_0 to $D^s(t = \infty)$.

5.5. Hydrodynamic considerations: perturbation of lipid flow

Membrane proteins affect the lipid solvent in (at least) two ways. First, they can perturb the flow of solvent; this phenomenon leads to hydrodynamic interprotein interactions. Second, they can perturb the conformation of individual lipid molecules, and thereby affect both the interprotein force and the bilayer viscosity. These two effects are considered in turn.

As currently presented, our model neglects hydrodynamic interactions. This interaction has, however, been extensively analyzed by theorists who primarily focus on three-dimensional diffusion (Faraday Division, 1983; Pusey and Tough, 1985; Faraday Division, 1987). In three-dimensional work, hydrodynamic effects are incorporated into the mathematical formalism by modifying the original generalized Smoluchowski equation for the time-dependent two-particle distribution function (Eq. A1). Specifically, the diffusion coefficient D_0 we are currently using is converted into a diffusion tensor $\tilde{\mathbf{D}}$. (Our D_0 can really be thought of as $D_0\tilde{\mathbf{I}}$, where $\tilde{\mathbf{I}}$ is the unit dyadic.) This diffusion tensor in general depends on the relative positions of all solute molecules in the system. Terms involving the hydrodynamic diffusion tensor must then be carried through the calculation and would ultimately appear in Eqs. 6–8 for the diffusion coefficient. We could, in principle, also generalize our description in this same way given an appropriate form for $\tilde{\mathbf{D}}$. However, to date a form for the hydrodynamic interaction tensor describing anisotropic motion in a membrane sheet surrounded by water has not been derived; hence we are content to discuss, for now, the results that have been obtained in the three-dimensional work.

It is generally felt that hydrodynamic effects are not particularly significant in dilute systems that interact through long-ranged potentials (Schurr and Schmitz, 1986). However, when the interparticle force is short-ranged, or when the solute concentration is high, hydrodynamics cannot be neglected. This observation about short-ranged, e.g., hard-core interactions, is particularly relevant because most of the available two-dimensional Monte-Carlo data (Pink, 1985; Saxton, 1987*a*) describe pure hard-disk systems. If the three-dimensional results provide a correct qualitative description of two-dimensional samples, the available hard-disk results may substantially overestimate the reduction in the self-diffusion coefficient. For example, it is known that for a dilute hard-sphere system in three dimensions $D^s/D_0 = 1 - 2f_v$ when hydrodynamics are neglected; the relevant expression is $D^s/D_0 = 1 - (0.2 \pm 0.1) f_v$ when hydrodynamics are incorporated into the description (Pusey and Tough, 1985). Here f_v is the volume fraction occupied by the solute. The effects of hydrodynamics on the longer-ranged 6-4 potentials are probably less pronounced, particularly at the lower densities.

An analysis of the role that hydrodynamic interactions play in membrane protein diffusion is an important goal of our future work.

5.6. Viscosity considerations: perturbation of lipid conformation

A considerable body of evidence supports the idea that membrane proteins perturb the conformation of the lipid solvent (Jost and Griffith, 1982; Watts and de Pont, 1985). Such perturbations affect the interprotein force and the membrane viscosity, and hence rates of diffusion.

Free-energy differences associated with protein-induced changes in lipid conformation can give rise to density-dependent, lipid-mediated, protein-protein interactions (see the review by Abney and Owicki [1985]). These interactions are easily incorporated into the diffusion theory if they are allowed to contribute to the total interprotein force. As mentioned previously, the attractions in the 6-4 fluid were meant qualitatively to model the effects of such interactions (although this force was not allowed to vary with density in our calculations).

Bilayer viscosity is also affected by lipid conformation (as well as by other factors). Typical microscopic diffusion theory, such as the Smoluchowski approach used here, does not include a description of perturbation in solvent structure. This is not an oversight, but rather reflects the fact that these theories are typically used to describe diffusion in an aqueous medium.

We could attempt to model the protein-induced changes in lipid conformation in the following fashion. Suppose that the conformational effects decouple completely from true direct and hydrodynamic interactions. We can then think of an ideal (noninteracting) protein and a conformationally perturbed lipid membrane which is characterized by a new viscosity. This new viscosity, of course, embodies the effect of changes in lipid structure. D_0 is then rescaled as prescribed, for example, by the Saffman-Delbrück equation, in a manner that reflects the new membrane viscosity. Finally, we allow the protein molecules to interact through direct and hydrodynamic forces and proceed with our Smoluchowski analysis as

before. The calculated D^s is now, however, referenced relative to the conformationally perturbed value of D_0.

The change in D^s induced by a conformational perturbation in viscosity is easily deduced. If structural changes increase (decrease) the viscosity, the decrease in the diffusion coefficient that originates from the direct interactions is augmented (counteracted). Unfortunately, it may not be easy to measure this conformational contribution to membrane viscosity. One could try to assay another, independent motion. However, viscosity refers to a particular dissipative mechanism and may not, therefore, be the same for two different molecules or even two distinct motions of the same molecule (Evans and Hochmuth, 1978; Schindler et al., 1980; Clegg and Vaz, 1985). In addition, protein concentration affects the motion of other molecules, e.g., lipids, in ways not directly connected to viscosity (Saxton, 1982; Eisinger et al., 1986; O'Leary, 1987; Saxton, 1987a).

5.7. Comparison with experiments on integral membrane proteins

Although much experimental attention has focused on measurement of the diffusion of integral membrane proteins, comparatively little effort has been directed at determining the concentration dependence of the diffusion coefficient. Thus it is that experimental diffusion coefficients, at multiple protein:lipid ratios, are available only for gramicidin (Tank et al., 1982) and bacteriorhodopsin (Peters and Cherry, 1982; Vaz et al., 1984). These values were extracted from FRAP studies of proteins reconstituted into simple, phosphatidylcholine bilayers.

Full comparison with the experimental results requires a value of D_0. Typically D_0 is unknown; nevertheless we can make contact with experiment if we plot D_0 against f_A on a log/log scale. In such a plot, D_0 shifts the results vertically but does not change their functional shape. This approach was taken by Saxton (1987*a*) when he compared the diffusion coefficients cited above with the theoretical hard-disk ratio $D^s(f_A)/D_0$. We do not repeat his analysis.[1] He found that the diffusion coefficients for these proteins fall off more rapidly with density than expected for particles interacting exclusively through excluded volume.

It would thus appear that factors other than simple excluded-volume interactions also act to reduce the diffusion coefficients. Some possibilities can be easily eliminated. For example, the measurements were performed on reconstituted systems that lack external biological constraints. In addition, protein aggregation is unlikely to be important in these systems, both because the studies were carried out under conditions that do not favor substantial aggregation, and because the diffusion of small protein clusters is not expected to differ significantly from the diffusion of monomers (Saffman and Delbrück, 1975, and related references).

Our discussion has suggested that appending additional, longer-ranged protein-protein interactions onto the hard-core repulsion could further reduce the diffusion coefficient. However, invoking the existence of such additional interactions is not justified in the case of bacteriorhodopsin because this protein is believed to interact primarily through excluded volume (Pearson et al., 1983). The interaction potential for gramicidin has not been measured.

As discussed in Section 5.4, hydrodynamic interactions have not been incorporated into the two-dimensional theories, and to that extent the theoretical descriptions are incomplete. However, it has been noted (Ohtsuki and Okano, 1982), for purely repulsive forces (such as excluded-volume interactions) acting in three dimensions, that the hydrodynamic and direct interparticle interactions produce opposing changes in diffusion coefficients. Thus, hydrodynamic effects are expected to raise D^s/D_0 toward unity and will not (at least for repulsive interactions) reconcile theory and experiment.

Of the factors we have discussed, a protein-induced increase in lipid viscosity remains as a mechanism that could act to retard the diffusion of bacteriorhodopsin and gramicidin. This mechanism has been suggested before (Cherry and Godfrey, 1981; Jacobson et al., 1981; Peters and Cherry, 1982; Saxton, 1987*a*). Unfortunately, for the reasons discussed in the previous section, we cannot, at present, give a quantitative description of this viscosity effect.

5.8. Comparison with experiments on membrane-bound antibodies

Another set of experiments has focused on the self diffusion of antibody molecules bound to lipid hapten in model membranes (Subramaniam et al., 1986; Tamm, 1988; Wright et al., 1988). These systems are representative of a larger class of phospholipid-anchored membrane proteins in which there is a small membrane-bound anchor and a larger extramembranous component present in the aqueous phase (Low and Saltiel, 1988).

The experimental protocol involved binding varied amounts of fluorescently labeled antibody to lipid hapten in supported monolayers and bilayers. Diffusion coefficients were determined by FRAP. Over the time scale of

[1]Saxton's analysis is based on Fig. 6 of his paper. We note that the area fractions corresponding to the gramicidin data in this figure were overestimated by a factor of two because dimerization of the gramicidin was neglected (Michael Saxton, personal communication). The correctly analyzed gramicidin data are in slightly poorer agreement with theory than those in Fig. 6; however, this fact does not alter Saxton's (or our) conclusions.

these experiments, it has been shown that the antibody mobility reflects the lateral redistribution of the antibody-hapten complex (Smith et al., 1979). The bare-diffusion coefficient of the complex is primarily determined by the diffusion coefficient of the lipid itself (Smith et al., 1979); this is a consequence of the negligible friction of the antibody in the aqueous phase (Tamm, 1988).

Experiments were performed at various surface concentrations of antibody. It was noted that as the concentration of antibody increased, its diffusion coefficient decreased. Aggregation, which can lead to the creation of larger, less mobile, populations, was invoked in the interpretation of some of these results. However, under conditions that favored monomeric complex, Tamm (1988) observed that "the antibody lateral diffusion coefficient decreases only two–three-fold when the antibody surface concentration is increased up to saturation."

It seems reasonable that interactions between the antibodies will modulate their rate of lateral diffusion. Unfortunately, a quantitative comparison between our theoretical results and the single-component experimental data is not possible because values of the surface concentration of antibody, at which diffusion coefficients were measured, were not determined. However, the general observation that diffusion coefficients change only a fewfold as the surface concentration is increased up to saturation is entirely consistent with our results. We note that in this system high area fractions may be attained with a minimal perturbation in membrane viscosity because the interacting species, antibody, is so much larger than the lipid hapten.

Finally, the antibody results may bear on the conclusions derived from FRAP experiments on integral membrane components. In a typical FRAP experiment, diffusive motion is followed by attaching a bulky fluorescently labeled antibody or lectin to the lipid or protein. If interactions with the extracellular matrix can be neglected, the presence of the label probably does not significantly influence the value of the diffusion coefficient in a very dilute system. However, large labels may interact with one another, even at relatively low concentrations of the tagged species, and thereby induce a fewfold reduction in the measured diffusion coefficient.

6. CONCLUSIONS

Perhaps the most important conclusion of this work is that the self diffusion of membrane proteins should be viewed as the diffusion of interacting particles. At the high lateral protein densities characteristic of biological membranes, interprotein interactions will surely influence diffusive behavior in a nontrivial way. Here we have, for example, demonstrated that direct interprotein interactions will produce a fewfold reduction in the self-diffusion coefficient when the protein concentration is increased from infinite dilution to physiological levels. This sort of interaction-induced effect has probably been observed experimentally in studies of protein diffusion in both model and cellular systems. In model systems, in particular, interactions are expected to play a dominant role in dictating the density dependence of protein mobility. In cellular systems, biological structures such as the cytoskeleton and the extracellular matrix act in conjunction with interprotein interactions to determine diffusive behavior.

In most instances, we find that it is not necessary to attribute a temporal (or spatial) dependence to the diffusion coefficient. The time-independent, long-ranged value is manifest in most cellular motions of interest and is measured by the standard FRAP experiment. However, it may be important to invoke the spatial dependence of D^s when describing motion over distance scales $\lesssim 10$ nm.

It is worth noting that interparticle interactions may significantly influence the diffusive motion of a protein species that is not itself present at high area fraction. In concentrated membrane systems, the motion of any given species will in reality be influenced by forces (e.g., excluded volume) arising from a variety of other molecules. It might, therefore, be more appropriate to think of diffusive behavior as being dictated by the effective excluded volume of the system. Multicomponent generalizations of the theory presented here might permit a more rigorous analysis of this point (Ohtsuki, 1983).

Finally, we do not feel it is justified, based on the scant experimental data available at this time, to make definitive statements about the agreement between theory and experiment. Instead, we note that a better understanding of interaction-dependent protein diffusion will inevitably develop as more systematic measurements are made on a variety of (well-understood) systems, and the theoretical analyses are generalized to include the effects of protein-induced changes in lipid flow and conformation.

APPENDIX A

In this Appendix, we establish a relationship between $P_2(\mathbf{r}, t)$ and the radial perturbation function, $p(r, \omega)$, defined in Eqs. 6 and 7; we also derive an equation from which $p(r, \omega)$ can be determined.

When inertial effects are neglected, $P_2(\mathbf{r}, t)$ will satisfy a generalized diffusion equation of the form (Ohtsuki, 1982)

$$\frac{\partial P_2(\mathbf{r}, t)}{\partial t} = D_0 \nabla \cdot \{[2\nabla_r + 2\beta \nabla_r u(r)] P_2(\mathbf{r}, t) - \beta \int [\nabla_1 u(s) - \nabla_2 u(q)] P_3(\mathbf{r}, \mathbf{s}, t)\, d\mathbf{s} + F_0 \beta \hat{\mathbf{e}}_0 P_2(\mathbf{r}, t) e^{i\omega t}\}. \quad \text{(A1)}$$

Here D_0 is the bare-diffusion coefficient of the solute, $\mathbf{q} = \mathbf{s} - \mathbf{r}$ as noted in the text, and $P_3(\mathbf{r}, \mathbf{s}, t)$ is a time-dependent three-particle distribution

function. Eq. A1 looks complicated; however, it can be made to resemble a more traditional diffusion equation of the form

$$\frac{\partial P_2(\mathbf{r}, t)}{\partial t} = -\nabla \cdot \mathbf{J} \tag{A2a}$$

if the generalized flux $\mathbf{J}$ is identified with the quantity

$$\mathbf{J} = -D_0\{[2\nabla_r + 2\beta\nabla_r u(r)]P_2(\mathbf{r}, t) - \beta \int [\nabla_1 u(s) - \nabla_2 u(q)]P_3(\mathbf{r}, \mathbf{s}, t)\, d\mathbf{s} + F_0\beta\hat{\mathbf{e}}_0 P_2(\mathbf{r}, t)e^{i\omega t}\}. \tag{A2b}$$

We solve Eq. A1, for $P_2(\mathbf{r}, t)$, by considering the linear response of the distribution functions to the imposition of the external force. In the absence of the force, the two-particle protein distribution is governed by the equilibrium radial distribution function $g(r)$; therefore, when the external field is present we assume that the molecular distribution can be written

$$P_2(\mathbf{r}_{1j}, t) = \rho^2 g(r_{1j})\,[1 + \gamma p(r_{1j}, \omega)\cos\theta_{1j}e^{i\omega t}]. \tag{A3}$$

Here γ is an expansion parameter that characterizes the strength of the external force (Ohtsuki, 1982), $p(r_{1j}, \omega)$ is the radial component of the perturbed distribution, and $\cos\theta_{1j}$, the angle between $\mathbf{r}_{1j}$ and $\hat{\mathbf{e}}_0$, describes the angular dependence of $P_2(\mathbf{r}_{1j}, t)$. Distribution functions that do not depend on the position of particle 1 are unperturbed to first order in γ.

To solve for $P_2(\mathbf{r}, t)$, we require (see Eq. A1) an expression for $P_3(\mathbf{r}, \mathbf{s}, t)$. We will write the time-dependent three-particle distribution function as the dynamical superposition of two-particle distribution functions, i.e., $P_3(\mathbf{r}, \mathbf{s}, t) = P_2(\mathbf{r}, t)P_2(\mathbf{s}, t)P_2(\mathbf{q}, t)/\rho^3$. However, the superposition approximation is not used for the equilibrium configurations. These statements are expressed mathematically in the relationship

$$P_3(\mathbf{r}, \mathbf{s}, t) = \rho^3 g^{(3)}(r, s, q) \cdot [1 + \gamma p(r, \omega)\cos\theta_{12}e^{i\omega t} + \gamma p(s, \omega)\cos\theta_{13}e^{i\omega t}]. \tag{A4}$$

If expressions A3 and A4 for P_2 and P_3 are inserted into Eq. A1 and the coefficients of each power of γ are equated, one obtains a hierarchy of equations that dictates the spatial dependence of the distribution functions. The zeroth-order relationship is just the equilibrium BGY equation (see Section 3.2.2.). The term that is linear in γ yields

$$\nabla_r \cdot \left\{[\nabla_r + \beta\nabla_r u(r)]g(r)p(r)\cos\theta_{12} - \frac{\beta\rho}{2}p(r)\cos\theta_{12}\int [\nabla_1 u(s) - \nabla_2 u(q)]g^{(3)}(r, s, q)\, d\mathbf{r}_3\right\} - \frac{\beta\rho}{2}\nabla_r \cdot \left\{\int [\nabla_1 u(s) - \nabla_2 u(q)]p(s)\cos\theta_{13}g^{(3)}(r, s, q)\, d\mathbf{r}_3\right\} - \frac{i\omega}{2D_0}g(r)p(r)\cos\theta_{12} = -\cos\theta_{12}\frac{dg}{dr}. \tag{A5}$$

The BGY equation tells us that the expression under the first divergence in Eq. A5 is simply $g(r)\nabla_r[p(r)\cos\theta_{12}]$ in disguise. The fundamental vector equation for $p(r)$ can therefore be written

$$\nabla_r \cdot \left\{g(r)\nabla_r(p(r)\cos\theta_{12})\right\} - \frac{\beta\rho}{2}\nabla_r \cdot \left\{\int [\nabla_1 u(s) - \nabla_2 u(q)]p(s)\cos\theta_{13}g^{(3)}(r, s, q)\, d\mathbf{r}_3\right\} - \frac{i\omega}{2D_0}g(r)p(r)\cos\theta_{12} = -\cos\theta_{12}\frac{dg(r)}{dr}. \tag{A6}$$

Eq. A6 can be reduced to an equation for the purely radial component of the perturbation function, $p(r)$, if the vector operators are rewritten in two-dimensional polar coordinates. One finds that

$$\frac{\cos\theta_{12}}{r}\frac{d}{dr}\left[rg(r)\frac{dp}{dr}\right] - \frac{\cos\theta_{12}}{r^2}g(r)p(r) + \frac{\beta\rho}{2}\nabla_r \cdot \left[\int \left\{\frac{du(s)}{ds}\hat{\mathbf{s}} - \frac{du(q)}{dq}\hat{\mathbf{q}}\right\}p(s)\cos\theta_{13}g^{(3)}(r, s, q)\, d\mathbf{r}_3\right] - \frac{i\omega}{2D_0}g(r)p(r)\cos\theta_{12} = -\cos\theta_{12}\frac{dg}{dr}. \tag{A7}$$

Our final task is to determine the divergence of the integral in Eq. A7. The algebra is somewhat tedious; however, if each of the vectors $\hat{\mathbf{e}}_0$, $\hat{\mathbf{s}}$ and $\hat{\mathbf{q}}$ is decomposed into its components along the unit vectors $\hat{\mathbf{r}}$ and $\hat{\boldsymbol{\theta}}$ and the divergence is computed in polar coordinates, it can be shown that the third term in Eq. A7 is equal to

$$\frac{\beta\rho}{2}\left[\cos\theta_{12}\frac{1}{r}\frac{d}{dr}\left(r\int\left\{\frac{du}{ds}\cos\theta + \frac{du}{dq}\cos\phi\right\} \cdot \cos\theta p(s)g^3(r, s, q)s\, ds\, d\theta\right) - \frac{\cos\theta_{12}}{r} \cdot \int\left\{\frac{du}{ds} - \frac{s}{q}\frac{du}{dq}\right\}\sin^2\theta p(s)g^{(3)}(r, s, q)s\, ds\, d\theta\right]. \tag{A8}$$

With this identification, we obtain Eq. 6; the angles are defined after Eq. 6 in the text.

APPENDIX B

Here we describe the conversion of continuum Eqs. 6 and 7 into discrete matrix form. The functions in Eqs. 6 and 7 were discretized using the same mesh (bin) size and lower and upper limits on r and s employed in the tabulation of $g(r)$ and $F(r, s)$; see Section 3.2. The discrete values of r and s, indexed below by i and j, respectively, were thus evenly spaced and separated by $\Delta = \Delta_r = \Delta_s$.

As noted in Section 3.3, setting $p(r, \omega) = p_r(r, \omega) + ip_i(r, w)$ separates Eq. 6 into two sets of coupled equations. In discrete form, these are

$$r_i^2 g(r_i)\frac{d^2p_r(r_i)}{dr^2} + \left[r_i^2\frac{dg(r_i)}{dr} + r_i g(r_i)\right]\frac{dp_r(r_i)}{dr} - g(r_i)p_r(r_i) + \frac{\rho\beta r_i}{2}\sum_j F(r_i, s_j)p_r(s_j)\Delta + \frac{\omega}{2D_0}g(r_i)p_i(r_i)r_i^2 = -r_i^2\frac{dg(r_i)}{dr} \tag{B1a}$$

and

$$r_i^2 g(r_i)\frac{d^2p_i(r_i)}{dr^2} + \left[r_i^2\frac{dg(r_i)}{dr} + r_i g(r_i)\right]\frac{dp_i(r_i)}{dr} - g(r_i)p_i(r_i) + \frac{\rho\beta r_i}{2}\sum_j F(r_i, s_j)p_i(s_j)\Delta - \frac{\omega}{2D_0}g(r_i)p_r(r_i)r_i^2 = 0. \tag{B1b}$$

Here the integrals were written, for r_i fixed, as Riemann sums.

Since we wanted to derive an equation for the perturbation function alone, the derivatives $dp(r)/dr$ and $d^2p(r)/dr^2$ were eliminated from Eq. B1; specifically, these derivatives were rewritten as weighted sums

of discrete values of $p(r)$ using a five-point least-squares fit to a quartic polynomial (Savitzky and Golay, 1964). Thus, we set

$$\frac{dp(r_i)}{dr} = \frac{1}{12\Delta}[p(r_{i-2}) - 8p(r_{i-1}) + 8p(r_{i+1}) - p(r_{i+2})] \quad \text{(B2a)}$$

and

$$\frac{d^2p(r_i)}{dr^2} = \frac{1}{12\Delta^2} \cdot [-p(r_{i-2}) + 16p(r_{i-1}) - 30p(r_i) + 16p(r_{i+1}) - p(r_{i+2})]. \quad \text{(B2b)}$$

Combining Eqs. B1 and B2 allowed us to rewrite Eqs. 6 and 7 as a single matrix equation of the form

$$\sum_k M_{ik}p_k = b_i. \quad \text{(B3)}$$

Here the $\{p_k\}$ represent ordered, discrete values of $p(r)$, first real and then imaginary, and the $\{b_i\}$ denote ordered, discrete values of the right-hand-sides of Eqs. B1a and b, first the $\{-r_i^2\, dg(r_i)/dr\}$ and then $\{0\}$. The $\{M_{ik}\}$ represent elements of the operator matrix; for an analysis based on n mesh points (bins), a matrix of $2n$ rows and columns resulted (n each from the real and imaginary terms). Many of these matrix elements are zero; two representative nonzero elements are given below:

$$M_{i,i-1} = \frac{16}{12\Delta^2} r_i^2 g(r_i) - \frac{8}{12\Delta} \cdot \left[r_i^2 \frac{dg(r_i)}{dr} + r_i g(r_i)\right] + \frac{\rho\beta r_i}{2} F(r_i, s_{i-1})\Delta, \quad \text{(B4)}$$

and

$$M_{n+i,i} = -\frac{\omega}{2D_0} g(r_i)\, r_i^2. \quad \text{(B5)}$$

To verify Eq. B4, note that $k = i-1$; hence, $M_{i,i-1}$ contains all terms in Eq. B1a (where the derivatives are evaluated using Eq. B2) that multiply $p_r(r_{i-1})$ or $p_r(s_{i-1})$. Similarly, Eq. B5 contains all the terms in Eq. B1b that multiply $p_r(r_i)$.

Boundary conditions were imposed by replacing the edge equations generated above by the likewise-linearized boundary conditions (each boundary condition contributed two equations as above, one in the real terms and one in the imaginary). Eq. 7a was implemented at a (large) value of r for which $du(r)/dr$ was zero (beyond the cutoff imposed on the analytical potentials). Eq. 7b was imposed at the hard-disk diameter for the excluded-volume interactions and at a (small) value of r for which $g(r) \approx 0$ for the extended potentials. In the latter case, the result was insensitive to the exact bin chosen as long as $g(r) \ll 1$.

Please note that the prescription given above does not apply to the first or last two columns. There different expressions must be used for the first and second derivatives (see Appendix 2 in Abney [1987]); however, the generalization is obvious.

We are pleased to acknowledge helpful conversations on various aspects of diffusion with Andrezj Altenberger, Daniel Axelrod, Aaron Kantor, Daniel Kivelson, George Phillies, Michael Saxton, Michael Schurr, Nancy Thompson, and Matthew Tirrell. We also received appreciated advice on mathematical and numerical points from Ole Hald, Karl Runge, and Richard Scalettar.

This work was funded in part by National Institutes of Health grant AI-22860 to John Owicki. Initial salary support to Bethe Scalettar was through National Institutes of Health grant GM30781 and United States Department of Energy grant DE-AC03-76SF00098 to John Hearst and Melvin Klein. James Abney and Bethe Scalettar are currently supported by appointments to the Alexander Hollaender Distinguished Postdoctoral Fellowship Program, supported by United States Department of Energy, Office of Health and Environmental Research, and administered by Oak Ridge Associated Universities.

Received for publication 8 June 1988 and in final form 6 December 1988.

REFERENCES

Abney, J. R. 1987. Protein-Protein Interactions in Membranes. Ph.D. Thesis, University of California, Berkeley.

Abney, J. R., and J. C. Owicki. 1985. Theories of protein-lipid and protein-protein interactions in membranes. *In* Progress in Protein-Lipid Interactions. A. Watts and J. J. H. H. M. de Pont, editors. Elsevier North-Holland Biomedical Press, Amsterdam. 1–59.

Abney, J. R., J. Braun, and J. C. Owicki. 1987. Lateral interactions among membrane proteins: implications for the organization of gap junctions. *Biophys. J.* 52:441–454.

Aloia, R. C. 1983–1985. Membrane Fluidity in Biology. Volumes 1–4. Academic Press Inc., New York.

Axelrod, D. 1983. Lateral motion of membrane proteins and biological function. *J. Membr. Biol.* 75:1–10.

Axelrod, D. 1985. Fluorescence photobleaching techniques and lateral diffusion. *In* Spectroscopy and the Dynamics of Molecular Biological Systems. P. M. Bayley, and R. E. Dale, editor. Academic Press, Inc., London. 163–176.

Beck, K. 1987. Mechanical concepts of membrane dynamics: diffusion and phase separation in two dimensions. *In* Cytomechanics. J. Bereiter-Hahn, O. R. Anderson, and W.-E. Reif, editors. Springer-Verlag GmbH & Co. KG, Heidelberg, Berlin. 79–99.

Bevington, P. R. 1969. Data Reduction and Error Analysis for the Physical Sciences. McGraw-Hill Book Company, New York.

Braun, J., J. R. Abney, and J. C. Owicki. 1984. How a gap junction maintains its structure. *Nature (Lond.).* 310:316–318.

Braun, J., J. R. Abney, and J. C. Owicki. 1987. Lateral interactions among membrane proteins: valid estimates based on freeze-fracture electron microscopy. *Biophys. J.* 52:427–439.

Bretscher, M. S. 1988. Fibroblasts on the move. *J. Cell Biol.* 106:235–237.

Chandler, D., J. D. Weeks, and H. C. Andersen. 1983. Van der Waals picture of liquids, solids, and phase transformations. *Science (Wash., DC).* 220:787–794.

Cherry, R. J., and R. E. Godfrey. 1981. Anisotropic rotation of bacteriorhodopsin in lipid membranes. *Biophys. J.* 36:257–276.

Clegg, R. M., and W. L. C. Vaz. 1985. Translational diffusion of proteins and lipids in artificial bilayer membranes: a comparison of experiment with theory. *In* Progress in Protein-Lipid Interactions. A. Watts and J. J. H. H. M. de Pont, editors. Elsevier North-Holland Biomedical Press, Amsterdam. 173–229.

Donaldson, P. K., and W. W. Webb. 1988. Monte Carlo simulation of concentration dependent lateral diffusion retardation requires intermolecular protein-lipid interactions *Biophys. J.* 53:121a. (Abstr.)

Dongarra, J. J., et al. 1979. LINPACK: Users' guide. Society for Industrial and Applied Mathematics, Philadelphia.

Edidin, M. 1987. Rotational and lateral diffusion of membrane proteins and lipids: phenomena and function. *Curr. Topics Membr. Transp.* 29:91–127.

Eisinger, J., J. Flores, and W. P. Petersen. 1986. A milling crowd model for local and long-range obstructed lateral diffusion: mobility of excimeric probes in the membrane of intact erythrocytes. *Biophys. J.* 49:987–1001.

Evans, E. A., and R. M. Hochmuth. 1978. Mechanochemical properties of membranes. *Curr. Topics Membr. Transp.* 10:1–64.

Faraday Division, Royal Society of Chemistry. 1983. Concentrated Colloidal Dispersions. *Faraday Discuss. Chem. Soc.* 76.

Faraday Division, Royal Society of Chemistry. 1987. Brownian Motion. *Faraday Discuss. Chem. Soc.* 83.

Forsythe, G. E., M. A. Malcolm, and C. B. Moler. 1977. Computer Methods for Mathematical Computations. Prentice-Hall, Englewood Cliffs, N.J.

Gumbiner, B., and D. Louvard. 1985. Localized barriers in the plasma membrane: a common way to form domains. *Trends Biochem. Sci.* 10:435–438.

Hackenbrock, C. R. 1981. Lateral diffusion and electron transfer in the mitochondrial inner membrane. *Trends Biochem. Sci.* 6:151–154.

Hill, T. L. 1956. Statistical Mechanics. McGraw-Hill, New York.

Hughes, B. D., B. A. Pailthorpe, and L. R. White. 1981. The translational and rotational drag on a cylinder moving in a membrane. *J. Fluid Mech.* 110:349–372.

Jacobson, K., Y. Hou, Z. Derzko, J. Wojcieszyn, and D. Organisciak. 1981. Lipid lateral diffusion in the surface membrane of cells and in multibilayers formed from plasma membrane lipids. *Biochemistry.* 20:5268–5275.

Jacobson, K., A. Ishihara, and R. Inman. 1987. Lateral diffusion of proteins in membranes. *Annu. Rev. Physiol.* 49:163–175.

Jost, P. C., and O. H. Griffith. 1982. Lipid-Protein Interactions. Vol. 2. John Wiley & Sons, New York.

Kell, D. B. 1984. Diffusion of protein complexes in prokaryotic membranes: fast, free, random or directed? *Trends Biochem. Sci.* 9:86–88.

Kubo, R. 1966. The fluctuation-dissipation theorem. *Rep. Prog. Phys.* 255:255–284.

Low, M. G., and A. R. Saltiel. 1988. Structural and functional roles of glycosyl-phosphatidylinositol in membranes. *Science (Wash. DC).* 239:268–275.

McCloskey, M., and M.-m. Poo. 1984. Protein diffusion in cell membranes: some biological implications. *Int. Rev. Cytol.* 87:19–81.

McQuarrie, D. A. 1976. Statistical Mechanics. Harper and Row, New York.

Metropolis, N., A. Rosenbluth, M. Rosenbluth, A. Teller, and E. Teller. 1953. Equations of state calculations by fast computing machines. *J. Chem. Phys.* 27:720–733.

Middlehurst, J., and N. S. Parker. 1986. Pair density distribution function of membrane particles at low density. *Biophys. J.* 50:1021–1023.

Ohtsuki, T. 1982. Dynamical properties of strongly interacting Brownian particles: II. Self-diffusion. *Physica.* 110A:606–616.

Ohtsuki, T. 1983. Dynamical properties of strongly interacting Brownian particles: III. Binary mixtures. *Physica.* 122A:212–230.

Ohtsuki, T., and K. Okano. 1982. Diffusion coefficients of interacting Brownian particles. *J. Chem. Phys.* 77:1443–1450.

O'Leary, T. J. 1987. Lateral diffusion of lipids in complex biological membranes. *Proc. Natl. Acad. Sci. USA.* 84:429–433.

Pearson, L. T., S. I. Chan, B. A. Lewis, and D. M. Engelman. 1983. Pair distribution functions of bacteriorhodopsin and rhodopsin in model bilayers. *Biophys. J.* 43:167–174.

Pearson, L. T., J. Edelman, and S. I. Chan. 1984. Statistical mechanics of lipid membranes: protein correlation functions and lipid ordering. *Biophys. J.* 45:863–871.

Peters, R. 1981. Translational diffusion in the plasma membrane of single cells as studied by fluorescence microphotolysis. *Cell Biol. Int. Rep.* 5:733–760.

Peters, R. 1985. Lateral mobility of proteins in membranes. *In* Structure and Properties of Cell Membranes. Vol. 1. Gh. Benga, editor. CRC Press, Boca Raton, Florida. 35–50.

Peters, R., and R. J. Cherry. 1982. Lateral and rotational diffusion of bacteriorhodopsin in lipid bilayers: experimental test of the Saffman-Delbrück equations. *Proc. Natl. Acad. Sci. USA.* 79:4317–4321.

Petersen, N. O. 1984. Diffusion and aggregation in biological membranes. *Can. J. Biochem.* 62:1158–1166.

Petersen, N. O., S. Felder, and E. L. Elson. 1986. Measurement of lateral diffusion by fluorescence photobleaching recovery. *In* Handbook of Experimental Immunology. Vol. 1. Immunochemistry. D. M. Weir, L. A. Herzenberg, C. Blackwell, and L. A. Herzenberg, editors. Blackwell Science Publishers, Palo Alto. 24.1–24.23.

Phillies, G. D. J. 1975. Fluorescence correlation spectroscopy and nonideal solutions. *Biopolymers.* 14:499–508.

Pink, D. A. 1985. Protein lateral movement in lipid bilayers. Simulation studies of its dependence upon protein concentration. *Biochim. Biophys. Acta.* 818:200–204.

Pink, D. A., D. J. Laidlaw, and D. M. Chisholm. 1986. Protein lateral movement in lipid bilayers: Monte Carlo simulation studies of its dependence upon attractive protein-protein interactions. *Biochim. Biophys. Acta.* 863:9–17.

Pusey, P. N., and R. J. A. Tough. 1985. Particle interactions. *In* Dynamic Light Scattering: Applications of Photon Correlation Spectroscopy. R. Pecora, editor. Plenum Publishing Corp. New York. 85–179.

Rallison, J. M., and E. J. Hinch. 1986. The effect of particle interactions on dynamic light scattering from a dilute suspension. *J. Fluid Mech.* 167:131–168.

Saffman, P. G. 1976. Brownian motion in thin sheets of viscous fluid. *J. Fluid Mech.* 73:593–602.

Saffman, P. G., and M. Delbrück. 1975. Brownian motion in biological membranes. *Proc. Natl. Acad. Sci. USA.* 72:3111–3113.

Savitzky, A., and M. J. E. Golay. 1964. Smoothing and differentiation of data by simplified least squares procedures. *Anal. Chem.* 36:1627–1639.

Saxton, M. J. 1982. Lateral diffusion in an archipelago: effects of impermeable patches on diffusion in a cell membrane. *Biophys. J.* 39:165–173.

Saxton, M. J. 1987*a*. Lateral diffusion in an archipelago: the effect of mobile obstacles. *Biophys. J.* 52:989–997.

Saxton, M. J. 1987*b*. Lateral diffusion in an archipelago: the distance dependence of the diffusion coefficient. *Biophys. J.* 51:542a. (Abstr.)

Scalettar, B. A., J. R. Abney, and J. C. Owicki. 1988. Theoretical comparison of the self diffusion and mutual diffusion of interacting membrane proteins. *Proc. Natl. Acad. Sci. USA.* 85:6726–6730.

Schindler, M., M. J. Osborn, and D. E. Koppel. 1980. Lateral mobility in reconstituted membranes—comparisons with diffusion in polymers. *Nature (Lond.)*. 283:346–350.

Schurr, J. M., and J. S. Schmitz. 1986. Dynamic light scattering studies of biopolymers: effects of charge, shape and flexibility. *Annu. Rev. Phys. Chem.* 37:271–305.

Shinitzky, M. 1984. Physiology of Membrane Fluidity. CRC Press, Boca Raton, Florida.

Singer, S. J., and G. L. Nicolson. 1972. The fluid mosaic model of the structure of cell membranes. *Science (Wash. DC)*. 175:720–731.

Smith, L. M., J. W. Parce, B. A. Smith, and H. M. McConnell. 1979. Antibodies bound to lipid haptens in model membranes diffuse as rapidly as the lipids themselves. *Proc. Natl. Acad. Sci. USA*. 76:4177–4179.

Subramaniam, S., M. Seul, and H. M. McConnell. 1986. Lateral diffusion of specific antibodies bound to lipid monolayers on alkylated substrates. *Proc. Natl. Acad. Sci. USA*. 83:1169–1173.

Tamm, L. K. 1988. Lateral diffusion and fluorescence microscope studies on a monoclonal antibody specifically bound to supported phospholipid bilayers. *Biochemistry*. 27:1450–1457.

Tank, D. W., E. S. Wu, P. R. Meers, and W. W. Webb. 1982. Lateral diffusion of gramicidin C in phospholipid multibilayers: effects of cholesterol and high gramicidin concentration. *Biophys. J.* 40:129–135.

Vaz, W. L. C., Z. I. Derzko, and K. A. Jacobson. 1982. Photobleaching measurements of the lateral diffusion of lipids and proteins in artificial phospholipid bilayer membranes. *In* Membrane Reconstitution. G. Poste and G. L. Nicolson, editors. Elsevier, North-Holland Biomedical Press, Amsterdam. 83–136.

Vaz, W. L. C., F. Goodsaid-Zalduonodo, and K. Jacobson. 1984. Lateral diffusion of lipids and proteins in bilayer membranes. *FEBS (Fed. Eur. Biochem. Soc.) Lett.* 174:199–207.

Watts, A., and J. J. H. H. M. de Pont, editors. 1985. Progress in Protein-Lipid Interactions. Elsevier North-Holland Biomedical Press, Amsterdam.

Wiegel, F. W. 1980. Fluid Flow Through Porous Macromolecular Systems. Lecture Notes in Physics. Vol. 121. Springer-Verlag Inc., NY.

Wright, L. L., A. G. Palmer III, and N. L. Thompson. 1988. Inhomogeneous translational diffusion of monoclonal antibodies on phospholipid Langmuir-Blodgett films. *Biophys. J.* 54:463–470.